Journal of Materials Chemistry B

PAPER

View Article Online
View Journal | View Issue

Cite this: J. Mater. Chem. B, 2019, 7, 6981

Ga and Ce ion-doped phosphate glass fibres with antibacterial properties and their composite for wound healing applications

Agata Łapa,[ab] Mark Cresswell,[b] Ian Campbell,[b] Phil Jackson,[b] Wolfgang H. Goldmann,[c] Rainer Detsch,[a] Andrew Parsons,[d] Ifty Ahmed[e] and Aldo R. Boccaccini *[a]

Novel gallium/cerium-doped phosphate glass fibres (PGF) were successfully manufactured by the melt-quenching and melt-spinning process. The amorphous character of the materials produced was confirmed using X-ray powder diffraction (XRD), and the elemental composition was investigated with X-ray fluorescence confirming the presence of 2 mol% of Ga_2O_3 or CeO_2. Fourier Transform Infrared Spectroscopy (FTIR) confirmed the presence of Q^1 and Q^2 structural phosphate species. Mechanical properties of the PGFs revealed tensile strength values of 428 ± 94 MPa and 379 ± 80 MPa, with elastic modulus values of 45 ± 4 GPa and 54 ± 9 GPa for Ce-PGF (diameter 25 μm) and Ga-PGF (diameter 18 μm), respectively. The influence of both dopants on the glass degradation properties was evaluated by tests in deionised water, which revealed a decreased dissolution rate for gallium-doped PGF in comparison to cerium-doped PGF. Inductively Coupled Plasma Optical Emission Spectroscopy (ICP-OES) measurements were used to explore ion release in cell culture medium, while ICP-mass spectrometry (ICP-MS) was used to measure ion release in deionised water. These techniques showed controlled release of therapeutic and antibacterial ions from the PGF. Antibacterial properties of Ce-PGF and Ga-PGF, based on turbidity measurements, were confirmed against Gram-positive bacteria. Moreover, Ce-doped phosphate glass fibres did not disturb the proliferation of human epidermal keratinocyte (HaCaT) cells or the mobility of mice embryonic fibroblasts (MEF). Applying an *in vitro* scratch assay showed full wound closure after 24 h of indirect incubation with Ga-PGF. Due to their superior processability as compared with Ga-PGFs, a fully degradable mesh based on Ce-PGF was designed and found to achieve high water uptake (up to 800%), suggesting its suitability for wound healing applications.

Received 27th April 2019,
Accepted 12th September 2019

DOI: 10.1039/c9tb00820a

rsc.li/materials-b

1. Introduction

Wound infections are a common problem associated with both acute (from burns) or chronic (*e.g.* foot ulcers or decubitus) wounds.[1] According to estimations around 1 to 2% of the population in developed countries will have to deal with a chronic wound during their lifetime.[2] The vast majority of novel wound dressings is based on polymers such as chitosan or alginate,[3] but there is a growing interest in applications of bioactive glass for wound healing applications.[4–6] Due to the brittle character of glass, especially promising are glass fibres due to their geometry, processability and flexibility.[7] In parallel, bacteria resistance to antibiotics has pushed scientists to look for drug-free strategies to fight infections.[8] Controlled release of ions with antibacterial capability is a promising solution to this complex problem. Ions such as silver (Ag)[9,10] and copper (Cu)[11,12] are known to be effective against Gram-positive and Gram-negative bacteria, however, some cytotoxic behaviour has been reported.[13] Two other elements with antibacterial properties, namely gallium (Ga) and cerium (Ce), are attracting interest, as they have also been shown to be beneficial due to their biological activity when in contact with mammalian cells.[14–17]

Due to their controllable degradation profiles, phosphate-based glasses (PBG) and phosphate glass fibres (PGF) are ideal platforms for tailored and controlled release of active ions,[14] in particular those known for their therapeutic properties.[18,19]

[a] Institute of Biomaterials, Department of Materials Science and Engineering, University of Erlangen-Nuremberg, Cauerstrasse 6, 91058 Erlangen, Germany. E-mail: aldo.boccaccini@fau.de
[b] Lucideon Ltd UK, Queens Road, Stoke on Trent ST4 7LQ, UK
[c] Department of Biophysics, University of Erlangen-Nuremberg, Henkestrasse 91, 91052 Erlangen, Germany
[d] Advanced Materials Research Group, Faculty of Engineering, University of Nottingham, University Park, Nottingham NG7 2RD, UK
[e] Composites Group, Faculty of Engineering, University of Nottingham, University Park, Nottingham NG7 2RD, UK

Moreover, the high solubility of PBG makes them suitable for both hard and soft tissue repair applications[20,21] such as muscle,[22] nerve[23] or skin regeneration.[12]

Gallium (Ga^{3+}) is an important element in bone growth, supporting hydroxyapatite formation.[24] It has been reported to inhibit the activity of osteoclasts and prevent bone resorption without having a negative impact on osteoblast activity.[25] Gallium has been approved by the FDA to treat hypercalcemia,[26] Paget's disease of bone, myeloma,[25] and autoimmune disease or allograft rejection.[15] Likewise, gallium therapies have shown effectiveness in bladder and urothelial carcinomas or lymphoma treatment.[15] The antibacterial properties of Ga have also been proven against both Gram-positive and Gram-negative bacteria.[27] Furthermore, studies have reported that resistance to antibiotics does not influence the antibacterial effectiveness of Ga^{3+} ions.[27] Gallium has a nearly identical ionic radius, coordination chemistry and ionisation potential as Fe(III)[27] and as such, it can act by an antibacterial mechanism known as the "Trojan horse strategy".[27] Several studies on phosphate-based glasses as Ga-delivery systems have been carried out,[28,29] as well as on Ga-containing silicate mesoporous bioactive glasses, borate glasses[16,30] and titanium implants.[31] The main reason behind incorporating gallium into a bioactive glass matrix is to exploit its antibacterial and biological properties. However, improvement in chemical durability of the parent borate glass has also been reported by addition of 5 wt% Ga_2O_3.[17]

Cerium (Ce^{4+}) has been shown to inhibit the growth of *Staphylococcus aureus* and *Escherichia coli*[32] due to its ability to dissociate the outer membrane of bacteria cells from the cytoplasmic membrane.[33] Cerium has been proposed to treat severe burns,[33] as nanoparticles of cerium oxide were shown to simulate fibroblasts, keratinocytes and vascular endothelial cells in a mouse wound model.[34] Several Ce-containing bioactive glasses for medical applications have been reported[35] due to the antibacterial capability and biological properties of cerium. Studies on bioactive silica glasses doped with Ce have shown cytocompatibility and effective interaction with L929 fibroblasts, whilst osteoblasts (MC3T3) have been reported to spread well on Ce-containing glass surfaces.[35]

In this study, a new family of gallium and cerium-doped phosphate-based glasses (PBG) has been manufactured and characterised to investigate the influence of these dopants on glass properties. Based on newly established compositions, two types of phosphate glass fibres (PGF) doped with gallium and cerium were obtained. A glass fibre mesh was also subsequently developed as a degradable dressing for wound healing applications and properties such as degradation and water uptake were also evaluated. Methylcellulose (MC) was used as the bonding agent to "glue" the fibres together forming a mechanically competent fibrous structure.

2. Materials and methods

Quaternary phosphate-based glasses of high magnesium content (A) and doped phosphate-based glasses (AGa, ACe) were manufactured using the melt-quench technique (Table 1).

Table 1 Nominal compositions of glasses A, ACe, AGa and reference phosphate glass fibres 40-PGF

A	$20MgO–11CaO–24Na_2O–45P_2O_5$ [mol%]
ACe	$18MgO–10CaO–24Na_2O–45P_2O_5–3CeO_2$ [mol%]
AGa	$18MgO–10CaO–24Na_2O–45P_2O_5–3Ga_2O_3$ [mol%]
40-PGF	$24MgO–16CaO–20Na_2O–40P_2O_5$ [mol%].

The powder precursors; calcium carbonate, sodium phosphate monobasic, magnesium phosphate dibasic trihydrate and mono-ammonium phosphate (Sigma Aldrich), and two antibacterial powder precursors; gallium oxide (Ga_2O_3) and cerium oxide (CeO_2) (Sigma Aldrich, Germany), were weighed (Ohaus Analytical plus, NJ, USA), mixed together, and sieved ($\varnothing$ 2 mm) to avoid any powder agglomeration. The sieving process was repeated two times in order to obtain the most homogeneous powder mixture. Powder glass batch was placed in a quartz crucible inside a pre-heated kiln at a temperature between 1100 and 1200 °C depending on the composition. After 1.5 h, the glass melt was poured onto a metallic plate in order to ensure rapid cooling and prevent crystallisation. The resulting glass frit was milled down to a powder (<150 μm) using a mortar and pestle.

2.1 Phosphate glass fibres

Phosphate glass fibres containing gallium or cerium (Ga-PGF and Ce-PGF) of the same chemical composition as AGa ($18MgO–10CaO–24Na_2O–45P_2O_5–3Ga_2O_3$ mol%) and ACe ($18MgO–10CaO–24Na_2O–45P_2O_5–3CeO_2$ mol%) shown in Table 1 were successfully drawn using a melt-spinning in-house designed fibre pulling rig.[36] 250 g of glass frit was placed inside the furnace and melted again at approximately 1000 °C. Once the viscosity was suitable, a fibrous filament exiting from the fibre bushing was pulled around a rotating drum (spinning at approximate rotation of 25–30 m s^{-1}). The glass fibres were then collected from the drum in order to investigate the biological and antibacterial role of ions (Ga^{3+} and Ce^{4+}), and an undoped glass fibre formulation (named P40) provided by University of Nottingham was used as a reference sample. The nominal composition of the undoped P40 glass was: $40P_2O_5–24MgO–16CaO–20Na_2O$ [mol%].

2.2 Ce-PGF mesh

Due to low processability of gallium-doped phosphate glass fibres (Ga-PGF), only cerium-doped fibres were used to manufacture random fibre mesh. Random fibre meshes were produced by manually cutting the long glass fibres (Ce-PGF) into short 0.5 cm lengths using scissors and mixing them with methylcellulose solution (2.5 g cellulose in 4 L of deionised water) using a magnetic stirrer for 10 minutes.[37] MC is non-toxic and does not cause an allergic reaction. Moreover, MC has been shown to possess good biocompatibility and has been used in traumatic brain injury and peripheral nerve regeneration.[38] In addition, methylcellulose is non-cell adhesive, which is an important factor in wound dressing as it allows for painless removal.[39] This solution was poured into another container, fitted with a sieve. The newly formed fibre mesh was collected with the sieve, rinsed with deionised water and placed for 24 h in a vacuum drier (Binder VOL115) at 50 °C.

2.3 Scanning electron microscopy (SEM)

SEM images of fibres (PGF) were obtained using a JEOL JSM-6490LV microscope fitted with an Oxford Instruments INCA Energy Dispersive X-Ray Analysis system (EDA). No sputter coating was applied before SEM examination. Imaging was conducted using Backscattered Electron Imaging; using this imaging mode the brightness of a given feature is proportional to its mean atomic number.

2.4 X-ray diffraction (XRD) analysis

Glass powder samples were measured using MiniFlex600 (Rigaku, Japan). The samples were continuously spun during data collection and scanned over a 2θ range of 20–80° using the conditions 0.02° per step and 4° min^{-1}.

2.5 X-ray fluorescence (XRF)

Samples were ground to a fine powder, and 0.05 g of material was then smeared onto a filter paper. This was then run on a Panalytical Axios XRF instrument using the applicable program for semi-quantitative analysis.

2.6 Fourier transform infrared spectroscopy (FTIR)

The nature of the bonding present in the powder samples was analysed using a FTIR-ATR spectrometer with diamond crystal (IRAffinity-1S, SHIMADZU, Japan). Each spectrum of glass sample was acquired and was averaged at resolution of 4 cm^{-1} over 20–40 scans and a range between 400 and 4000 cm^{-1}. The peak analysis was done using Origin 9.0 (OriginLab, USA) software.

2.7 Degradation test of PBG

Degradation tests were performed by placing 0.4 g of glass fibre samples into glass bottles with 40 ml of deionised water. Deionised water was chosen as the medium as it does not contain other ions that could influence degradation rate and ion release. Samples were incubated at 37 °C under dynamic conditions (shaking at 125 rpm). Every 7 days, the samples were filtered to remove water, washed with deionised water and dried in an oven at 37 °C overnight. The dry mass of the sample was measured using a laboratory balance (Ohaus Analytical plus, NJ, USA).

Percentage of dry mass was calculated according to eqn (1):

$$\%_{\text{dried mass}} = \frac{m_{\text{dried}}}{0.4} \times 100\% \quad (1)$$

where m_{dried} is the mass of the sample after drying, and 0.4 is the mass of the initial sample [gram].

2.8 Inductively-coupled plasma mass spectrometry

To prepare samples for ICP-MS analysis, 0.4 g of glass fibres were measured and incubated in 40 ml deionised water at 37 °C under dynamic conditions (shaken at 125 rpm). After 1, 24 and 48 h, 1 ml aliquots were taken from each solution and diluted 20 times. Samples were then analysed using an Agilent Technologies 5110 DV instrument. The results obtained in ppm (parts per million) were calculated and presented as a percentage of total glass mass. The aqueous samples were analysed by using an Agilent 7900 ICP-MS instrument.

2.9 Inductively-coupled plasma optical emission spectrometry

ICP-OES analysis of glass powder samples (1 wt/vol%) incubated in CCM (Cell Culture Medium contains: RPMI/DMEM + 10 vol% fetal bovine serum + 1 vol% penicillin streptomycin solution Gibco, Sigma Aldrich, Germany) at 37 °C was conducted predominantly using helium as the collision gas to remove polyatomic (oxide-based) mass interferences by kinetic energy discrimination (KED). In some cases, such as for calcium determination, analyses were also conducted using hydrogen reaction gas to remove doubly-charged mass interferences by charge transfer. The raw counts for each analytical mass were translated into concentration by the Agilent MassHunter software after a multi-point calibration with linear fit ($r^2 > 0.999$). Over-range samples were diluted in a 2% nitric acid matrix to match the calibration standards.

2.10 Single fibre tensile test (SFTT)

Mechanical tests were carried out using a Single Fibre Tensile Test (SFTT) machine according to ISO 11566 as described elsewhere.[40] Single fibre filaments were glued onto a plastic plate using acrylic adhesive and cured with UV light. Every filament was measured using a laser scanning micrometer LSM 6200 (Mitutoyo, Japan) to determine the fibre diameter. The LSM 6200 was calibrated by using glass filaments of known diameters measured *via* SEM imaging. Mechanical properties were measured using a LEX810 Tensile Tester (Dia-Stron, UK) at room temperature with a load capacity of 20 N and a speed of 0.017 mm s^{-1}.

2.11 Water uptake

Water uptake of the glass fibre/methylcellulose meshes was measured by comparing the dry mass of the samples with the wet mass after different incubation times (5 min, 15 min, 1 h, 24 h and 48 h) in deionised water, according to eqn (2).[41]

$$\text{Water uptake } (\%) = \frac{\text{dry mass} - \text{wet mass}}{\text{dry mass}} \times 100\% \quad (2)$$

The measurements were performed in triplicate.

2.12 Viability assay of HaCaT cells in indirect contact with phosphate glass fibres

Human epidermal keratinocytes (HaCaT) were maintained as monolayer in cell culture medium containing as follows: Dulbecco's Modified Eagle Medium (DMEM) with high glucose (Sigma Aldrich, Germany), 10 vol% fetal bovine serum (Sigma Aldrich, Germany) and 1 vol% penicillin–streptomycin (Sigma Aldrich, Germany). Cells were incubated at 37 °C in a humidified atmosphere of 5% CO_2 in air. 1 wt/vol% of chopped phosphate glass fibres (Ce-PGF, Ga-PGF and undoped 40-PGF) were incubated for 24 h in cell culture medium, later the supernatants were filtered to remove the remaining fibres. 5000 cells per ml were placed in a 48-well plate and incubated for 6 h. Later, when cells had attached

to the bottom, the medium was removed and replaced with the supernatants. 5 vol% solution of WST-8 (tetrazolium salt) in CCM was used to measure viability of the cells after 1, 2, 5 and 7 days. Standard cell culture medium was used as a control (standard cell culture), and tests were run on 6 replicas.

2.13 Wound closure *in vitro*

To investigate the influence of Ce-PGF on fibroblast behaviour, an *in vitro* scratch assay was applied according to a previously reported protocol.[42]

Mouse embryonic fibroblasts (MEF, Sigma Aldrich, Germany) were used. 0.1 g of Ce-PGF and 0.1 g of 40-PGF (undoped phosphate glass fibres) were sterilised using the dry heat method (2 h at 160 °C) and incubated separately in 10 ml of cell culture medium (CCM) for 24 h at 37 °C. CCM contains MEM-α medium (Gibco, Germany), 10 vol% fetal bovine serum (Sigma Aldrich, Germany) and 1 vol% of penicillin streptomycin solution (Sigma Aldrich, Germany). After 24 h of incubation, the supernatant at concentration of 1 wt/vol% was collected and diluted 10×, which allowed to obtain two concentrations of 1 wt/vol% and 0.1 wt/vol%. MEF cells were seeded onto the 24-well plates (100 000 cells per ml, 1 ml per well) and incubated for 24 h at 37 °C.

After 24 h, once the cells had attached to the bottom of the wells, a scratch was made using a p200 sterile pipet tip in every well. The medium was removed, and all wells containing cells were washed with DPBS (double phosphate buffered saline, Sigma Aldrich, Germany). Later, DPBS was removed and replaced by the supernatant (1 and 0.1 wt/vol%). On the outer part of the well plates, a scratch was made using a scalpel to mark the scratch in the fibroblast layer.

The migration of fibroblasts and *in vitro* wound closure were monitored by light microscope (AxivoVert) at the following time points after formation of the scratch: 0, 4, 6, 8 and 24 h. The gap between the edges of MEF layers (the width of scratch) was measured using ImageJ.

2.14 Turbidity measurements

Both colonies *Escherichia coli* (Gram-negative bacteria) and *Staphylococcus carnosus* (Gram-positive bacteria) were transferred and incubated in a shaker separately in 10 ml of LB-medium (Luria/Miller medium, Carl Roth, Germany) for 24 h at 37 °C. After 24 h, the necessary volume [μl] of bacteria broth was added to 1 ml of bacteria free-medium to evaluate the exact volume of bacteria broth that allows an optical density (OD) equal to 0.015 at a wavelength of 600 nm in the photometer. The volume depends on the bacteria growth, however, in this experiment 10 μl of bacteria broth gave 0.015 (OD) in 1 ml of 1 ml bacteria-free medium. Subsequently, 0.1 g of each glass fibre was added to a 24-well plate followed by 2 ml of medium to obtain a 5 wt/vol% concentration. Later, 20 μl of bacteria broth was added obtaining an OD of 0.015 for each sample.[43] Similar well plates were prepared for both Gram-positive and Gram-negative bacteria and incubated for 48 h. The optical density of each sample (3 replicas) was measured after 4, 24 and 48 h. A control used in this experiment was a bacteria broth not exposed to the glass fibres.

The turbidity measurement is a sensitive method,[44] which allows detection of even low differences based on light scattering by bacteria.[45] The technique measures the optical density at 600 nm and was developed to monitor the bacteria growth in liquid media over time in an easy and low-cost way. Recently, it has been used to evaluate the antibacterial properties of biomaterials. The OD measurement allows calculation of the relative bacterial viability%,[46] as follows:

$$\text{Relative bacterial viability}\% = \frac{\text{sample OD}}{\text{blank control OD}} \times 100\% \quad (3)$$

2.15 Statistical analysis

All results are expressed as mean ± standard deviation. Statistically significant differences have been assessed, using one-way ANOVA to compare (Bonferroni comparison) multiple datasets ($p < 0.05$).

3. Results and discussion

3.1 Scanning electron microscopy

A SEM image showing the morphology of PGF (undoped) is presented on Fig. 1. Phosphate glass fibres are continuous, and uniform exhibiting smooth surfaces and diameters in the micrometre range. The appearance of PGF corresponds to other fibres reported in the literature and there was no difference in the macroscopy appearance of the different fibres investigated in this study.

3.2 X-ray fluorescence

The chemical composition of the PBG and PGF was measured using XRF. The results showed some silica contamination, which likely came from the quartz crucible in which the glass was melted. The nominal (planned) compositions are given in Table 1 and for convenience are provided again with the XRF data in Table 2. The process of pulling the glass fibres is not expected to change the chemical composition of the fibres, thus Ce-PGF and Ga-PGF were expected to have the same composition as ACe and AGa bulk glass, respectively.

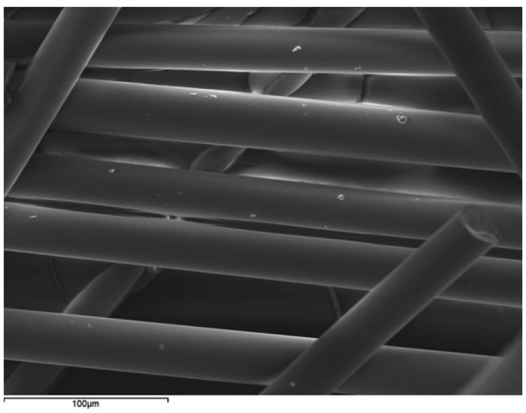

Fig. 1 SEM image of undoped PGF showing continuous and uniform surface.

Table 2 Nominal and empirical compositions (measured by XRF) of glasses A, ACe and AGa

Glass	Composition [mol%]
A	Nominal: $20MgO–11CaO–24Na_2O–45P_2O_5$
	Empirical (XRF): $18MgO–11CaO–27Na_2O–41P_2O_5–3SiO_2$
ACe/Ce-PGF	Nominal: $18MgO–10CaO–24Na_2O–45P_2O_5–3CeO_2$
	Empirical (XRF): $18MgO–10CaO–25Na_2O–42P_2O_5–3SiO_2–2CeO_2$
AGa/Ga-PGF	Nominal: $18MgO–10CaO–24Na_2O–45P_2O_5–3Ga_2O_3$
	Empirical (XRF): $17.5MgO–11CaO–24Na_2O–43.5P_2O_5–2SiO_2–2Ga_2O_3$

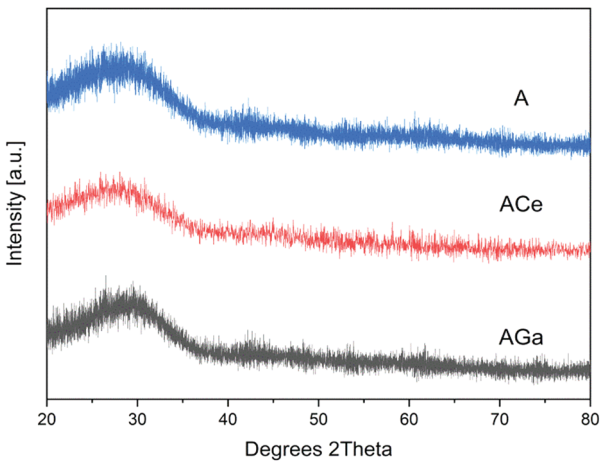

Fig. 2 XRD spectra of PBG powders confirming the amorphous character of all samples.

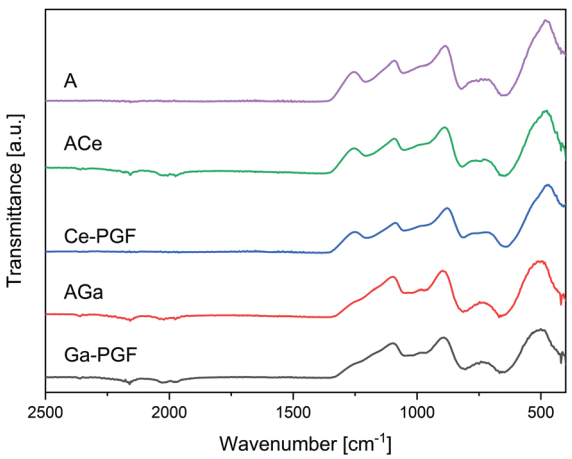

Fig. 3 FTIR spectra of doped PBG powders (A, AGa and ACe) and powders from doped PGF. Characteristic peaks are presented in Table 3.

3.3 X-ray powder diffraction (XRD)

XRD spectra of powders of A, AGa and ACe glasses are presented in Fig. 2. The amorphous character of the samples is confirmed by the absence of crystallisation peaks in the spectra. The obtained glasses were transparent, and no crystallization could be observed. Phosphate glass fibres were manufactured based on glasses AGa and ACe.

3.4 Fourier-transform infrared spectroscopy

FTIR spectra of powders obtained from doped PBG and PGF are shown in Fig. 3, and the main peaks observed are summarized in Table 3. Peaks around 480 cm^{-1}, 756 cm^{-1}, 900 cm^{-1} and 1100 cm^{-1} were observed for all glass compositions, suggesting the presence of Q^1 and Q^2 units associated with P–O bonds.[48] Gallium-doped glasses show reduction of the peak around 1250 cm^{-1}, as well as shifts to higher wavenumbers for all peaks. Glass AGa and the corresponding Ga-PGF (doped with gallium) and ACe and Ce-PGF (doped with cerium) showed very similar peaks, suggesting that the bulk and fibre morphologies in essence retained similar structures.

Gallium oxide is an intermediate oxide that can play a role both as glass former and as a glass modifier oxide.[49] As such, Ga can increase connectivity in the glass network of phosphate glasses,[50] creating relatively strong covalent Ga–O–P bonds if it enters the glass-forming phosphate chain network. However, as an intermediate oxide it could also behave as a cross-linker between two phosphate chains. Additionally, the presence of Ga can lead to formation of Ga–O–Ga bonds that can stabilize the glass structure and increase durability.[51] Aluminium oxide, similar to gallium oxide[52] is also an intermediate oxide and its addition to PGFs can significantly enhance the chemical durability and mechanical properties of the fibres.[49]

Cerium is a glass modifier oxide, crosslinking the glass network.[53] However, cerium can exist in two oxidation states Ce^{3+} and Ce^{4+}, and the relative Ce^{3+}/Ce^{4+} ratio in our glass is unknown. Literature shows differences in the glass structure considering that as Ce^{4+} has higher field strength, shorter Ce–O bonds and lower oxidation states than Ce^{3+}, allowing for the creation of stronger bonds.[54] Increase of Ce^{3+} over Ce^{4+} causes weakening of the binding of bridging-oxygen and the strengthening of non-bridging oxygen.[53] However, the overall impact on the dissolution rate, described in the next section, is not conclusive.

Table 3 Interpretation of FTIR peaks of spectra shown in Fig. 3

Measured wavenumbers [cm^{-1}]	Interpretation
476–484	Attributed to the deformation modes of phosphate tetrahedral and vibration of cation oxygen polyhedron[47]
731–748	Symmetric stretching mode of the non-bridging oxygen stretching modes vibrations bonds Q^1 species[47]
885–889	Symmetric stretching vibration of P–O–P linkages in Q^2 [47]
1092–1097	Asymmetric stretching mode of the non-bridging oxygen stretching modes vibrations bonds Q^1 species[47]
1254–1256	Asymmetric stretching vibration of P–O–P linkages in Q^2 species[47]

According to the literature, introduction of cerium ions can increase the relative amount of Q^2 species, making the glass more hydrolytically resistant *vs.* non-doped compositions (that contains Q^3 units), due to formation of strong P–O chains with P–OH hydrogen bonds.[55] However, FTIR analysis did not confirm the presence of Q^3 units in our glass. In contrast, Lai *et al.*[47] stated that increase in Ce content leads to an increase in Q^2 species and an increase in T_g due to the effect of shorter and stiffer Q^2 chains. It is likely that shorter phosphate chains are hydrated and solubilized much quicker than longer phosphate chains, which could explain the enhanced dissolution rate. Additionally, decrease in Q^1 and increase in Q^2 are accompanied by the formation of Q^0 ($2Q^1 \leftrightarrow Q^2 + Q^0$ [47]), and this effect could possibly explain the increase in dissolution rate.

Structural analysis was not pursued further because the focus of this investigation was on the biological antibacterial properties of the new fibres, however, further studies (solid state ^{31}P NMR, XPS, *etc.*) would be required to fully confirm the initial observations as well as to evaluate the oxidation state of Ce.

3.5 Dissolution behaviour

Dissolution rates of doped-phosphate glass fibres are presented in Fig. 4. The cerium-doped glass fibres showed a significant decrease in dry mass after 1 day immersion in deionized H_2O and after it had dissolved completely after 7 days. On the other hand, Ga-PGF showed resistance to hydrolytic attack with 80% of dry mass remaining after 10 days of incubation in deionized water and decreasing to 25% after 28 days.

The dissolution rate of the phosphate glass fibres is different from that of the bulk glasses due to their specific geometry and higher surface area.[56] Ce-PGF have a low resistance to degradation in water, with 60% dissolving in the first 24 h of incubation, and then completely dissolving after 7 days. The diameter of Ce-PGF was significantly higher than that of Ga-PGF, which should also result in a comparatively lower degradation rate. The high degradation rate is in agreement with the ion release results presented in Fig. 5 (Section 3.5). Between 30–60% of the release from Ce-PGF occurs from 1 to 24 h, while ion release from Ga-PGF is linear and does not change significantly within the first 24 h.

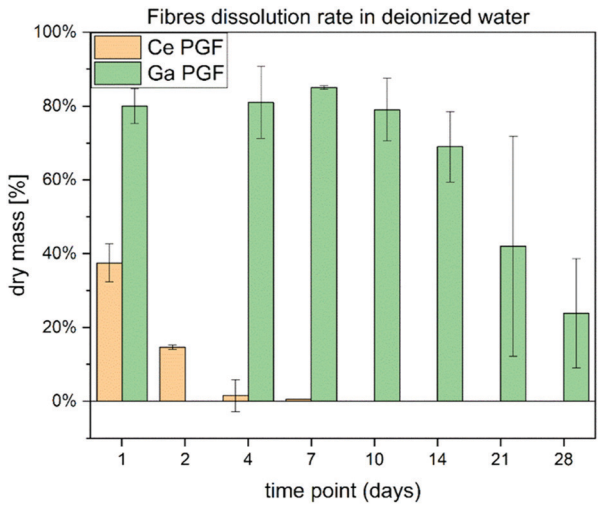

Fig. 4 Dissolution rate in deionised water of Ce and Ga-doped phosphate glass fibres over 28 days.

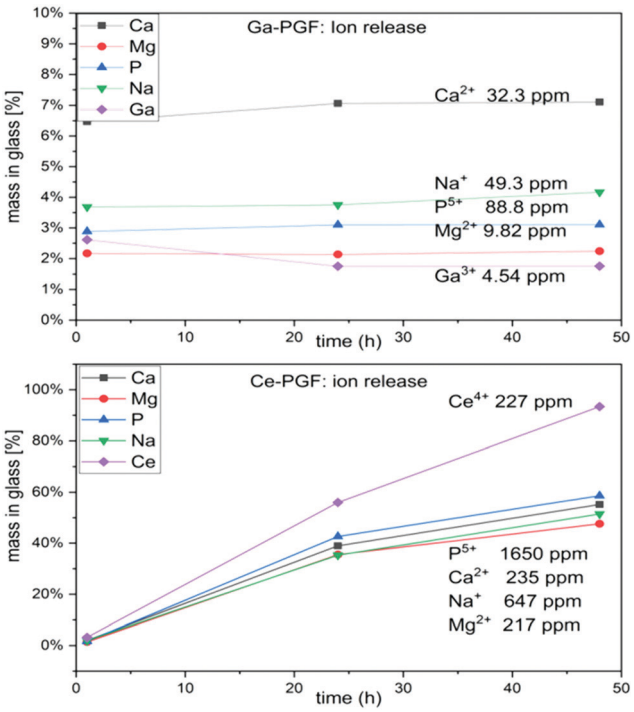

Fig. 5 Ion release (Ca, Mg, P, Na, Ce and Ga) during 48 h of incubation of Ga-PGF and Ce-PGF in deionised water.

The high degradation rate of Ce-PGF is potentially an effect of the composition and residual stress from the fibre drawing process. It has been shown that alleviating residual stresses by annealing can reduce solubility of the glass.[40] Additionally, the fibre pulling process could have affected the structure of Ce-PGF causing the decrease in chemical durability, which has been confirmed by high release of cerium ions. The fibre-drawing process leads to structural anisotropy due to alignment of the phosphate chains along the main axis, which may result in breaking up the lateral bonds as well as long chains.[40] However, based on FTIR analysis no significant differences between Ce-doped phosphate glass fibres *vs.* Ce-doped phosphate glasses were observed (Fig. 3).

Gallium oxide, behaving similarly to Al_2O_3, Fe_2O_3 or B_2O_3, can enter the phosphate chain backbone leading to the strengthening of the glass network and lowering of the degradation rate.[40,49,57] Fe_2O_3 can form a tetrahedral or octahedral coordination, acting as glass former as well as glass modifier,[57] and structural similarities between gallium and iron are stated in the literature.[26] Moreover, NMR analysis showed that Ga^{3+} is octahedrally coordinated by oxygen atoms, which increased durability of the glass.[14] On the other hand, structural anisotropy provides improved tensile strength and Young modulus of PGF,[40] which corresponds to the results presented in Section 3.7. Mechanical testing confirmed that the elastic modulus of

gallium-doped fibres was higher than that of the cerium-doped fibres.

3.6 Ion release

The ion release (over 48 hours) from Ce-PGF and Ga-PGF was measured from ion concentrations in deionized water and cell culture medium aliquots using both ICP-OES and ICP-MS methods.

The results of ion release from PGF are presented in Fig. 5. The lowest ion release was measured for Ga-PGF, which also revealed the lowest mass loss compared to the other samples. The fastest ion release was reported for Ce-PGF, which degraded entirely after 7 days (15% of dry mass remained after 2 days). High dissolution rates of Ce-PGF correlated with the high release of all ions, especially cerium ions (after 2 days almost 100% of Ce has been released). In contrast, release of the antibacterial dopant (gallium) was much lower (long-term release), which also correlated with the degradation profiles. Moreover, addition of gallium decreased the release of other ions present in the glass, as these formulations were much more stable to degradation. A similar effect has been reported by Sahdev *et al.*,[50] where an increase of gallium oxide in PBG led to a decrease in the release of other ions as well as overall dissolution. Addition of Ga^{3+} increased the connectivity of the glass network,[58] while degradation of gallium-doped phosphate-based glasses led to formation of gallium orthophosphates. In all samples, the plateau has been reached after 24 h.

To investigate the amount of ions released after 24 h of incubation of PGF in Cell Culture Medium (CCM, used in indirect cell test), ICP analysis of Ce-PGF, Ga-PGF, and 40-PGF was performed. The results are presented in Table 4. CCM contains ions (Na, Mg, P, Ca) that are present in the investigated samples. The difference in measured values suggests remineralization on the surface of glass fibres which has been reported before for bioactive glasses, however this possible effect was not further elucidated in the present study.

3.7 Mechanical properties of phosphate glass fibres

Mechanical properties of phosphate glass fibres (Ce-PGF and Ga-PGF) were measured using the Single Fibre Tensile test (SFTT) machine. The tensile strength and elastic modulus were 428 (±94) [MPa] and 45 (±4), 379 (±80) and 54 (±9), for Ce-PGF (diameter 25 ± 3 [μm]) and Ga-PGF (diameter 18 ± 2 [μm]), respectively.

The values obtained are characteristic for phosphate glass fibres that have been utilized as reinforcement in biocomposite applications, with values in the range 318–484 MPa (tensile strength) and 50–75 GPa (elastic modulus).[40] Unfortunately, the direct comparison of the effect of gallium and cerium on the mechanical properties is difficult due to the difference in the average diameter of the fibres (18 and 25 μm). Nevertheless, mechanical properties of phosphate-based glasses doped with trivalent ions such as B, Fe, and Al have shown increases in mechanical properties in comparison to undoped PGF.[22] The significantly lower dissolution rate of gallium-doped glass fibres may suggest improved mechanical properties of Ga-PGF over Ce-PGF, however a dedicated study should be conducted in future to assess quantitatively the effect of ion doping on mechanical properties of PGF.

Ahmed *et al.* have shown a doubling in elastic modulus and flexural strength by incorporating chopped PGF into PLA (elastic modulus increased from 2.5 to 5 GPa, flexural strength from 50 to 90 MPa).[59] Improved tensile strength in combination with antibacterial properties could allow further expansion of the application of phosphate-based glasses (for *e.g.* in developing biocomposite fracture fixation devices).

3.8 Biological properties of phosphate glass fibres

Two biological tests were performed on PGF to investigate their possible application as a wound dressing. In these studies, the cells were not in direct contact with the surface of the fibres as the main focus was to investigate the effect of ion release on cell behavior and cytotoxicity and not to assess other variables such as the surface topography and morphology of the tested materials.

3.8.1 Viability assay of HaCaT cells in indirect contact with phosphate glass fibres. The viability of HaCaT cells was presented as a percentage of positive control in standard cell culture (Fig. 6). After 1 day of incubation, the values of proliferation were nearly the same for cells exposed to all supernatant. After day two, the values measured for the control and the cells incubated with the supernatant were significantly different suggesting the influence of the ions released from the PGF samples on cell proliferation. A similar trend was observed after 5 days. On day 7, all the measured values were nearly identical (control, and supernatant of Ce-PGF, Ga-PGF, 40-PGF).

The supernatant of 40-PGF enhanced the viability of cells after the second and fifth day compared to the control, which persisted after the seventh day. The ICP measurement showed the release of Mg, Ca and Na ions, which are known to enhance the cell response.[18,19] Also, magnesium-based phosphate glass fibres were reported to have a positive influence on soft tissue regeneration.[21] Viability of cells slowed down after 5 days of incubation with Ga-PGF, which could be explained by the release and amount of gallium ions (5.25 mg l^{-1}). However, the number of cells was similar to the positive control after 7 days. Despite the

Table 4 Ion release after 24 h of incubation of PGF in cell culture medium. Relative Standard Deviation (RSD) for measured elements in CCM: 6.02% (Na), 5.11% (Mg), 2.61% (P), 1.72% (Ca), 2.71% (Ga), 1.35% (Ce)

	Sample	Na [mg l^{-1}]	Mg [mg l^{-1}]	P [mg l^{-1}]	Ca [mg l^{-1}]	Ga [mg l^{-1}]	Ce [mg l^{-1}]
Phosphate glass fibres	40-PGF	3161	19.7	28.0	72.3	0.15	0.00
	Ce-PGF	3175	99.4	536	116	0.47	**25.0**
	Ga-PGF	2770	27.3	56.1	76.1	**5.25**	0.03
Cell culture medium		3059	21.1	34.9	82.5	0.00	0.00

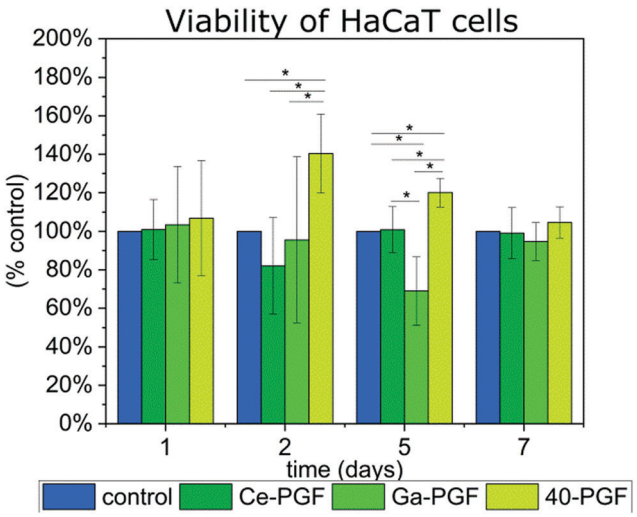

Fig. 6 Viability of HaCaT cells in indirect test with gallium/cerium-doped phosphate glass fibres over 7 days, results are presented as percentage of positive control (100%).

high release of cerium ions from Ce-PGF (25 mg l^{-1}), the sample did not show toxicity during the test. The values measured correspond to those of the control. This result is in agreement with literature, as Singh *et al.*[60] showed that cerium nanoparticles did not affect cellular metabolic activity of HaCaT cells at concentrations up to 0.1 mg ml^{-1} over four tested concentrations: 1 mg ml^{-1}, 0.1 mg ml^{-1}, 0.01 mg ml^{-1} and 0.001 mg ml^{-1}. However, in those studies, in 0.1 mg ml^{-1} (100 mg l^{-1}), a reduction in cell viability by 50% was reported. Small differences between day 1 and day 7 could be explained by too low and too high number of cells estimated on that specific day. The doubling time is known to be 24 h, which could cause confluency after 7 days of incubation (expected number of cells for positive control after 7 days is ~640 000 cells per well). HaCaT is an immortal cell line from adult human skin that is characterized by normal differentiation providing a promising platform to investigate cell behaviour in contact with biomaterials.[61] Moreover, cytocompatibility of phosphate-based glasses doped with molybdenum have also been tested using HaCaT cells, showing good cell viability.[62]

3.8.2 Wound closure *in vitro*. The *in vitro* scratch assay (wound closure *in vitro*) is a straightforward and inexpensive way to mimic the behaviour of a wounded cell layer in contact with the tested material.[42] It allows not only investigation of the time needed for full wound closure but also to observe cell migration (Fig. 7). Wound healing is a complex process, which requires both migration and proliferation of the cells.[63] The mobility of cells is driven by growth factors and cytokines[63] and depends on the cell type.[64] The ability to monitor, both cell migration and proliferation in real time, enables better understanding and prediction of the behaviour of the material in the real wound.

In vitro scratch assay was performed using the supernatant of Ce-PGF only to investigate possible behaviour of the random mesh as a soluble dressing.

Based on the microscopy images at 0, 4, 6, 8 and 24 h of scratch test, the gap distance (scratch width) was measured using ImageJ software. The average was calculated, which provided the percentage of wound closure at a given time point (Table 5). Almost 50% wound closure was measured after 8 h and full closure after 24 h in contact with the supernatant of Ce-PGF (1 wt/vol% and 0.1 wt/vol%).

In vitro scratch assay performed on supernatant of Ce-PGF did not show a significant difference between the 1 wt/vol%, 0.1 wt/vol% and control (standard cell culture). The supernatant of Ce-PGF showed non-toxicity and did not disturb cell migration and proliferation, leading to full wound closure after 24 h. Cell migration can be seen for all samples. The relatively high standard deviations presented in Table 5 correspond to the large spread of the values observed in Fig. 7. Indeed, when the cells started to migrate the shape of the gap changed from regular (two parallel lines) to irregular (zig-zag like) which made the measurement difficult. The values presented in Table 5 are the average size of the gap (scratch).

3.9 Antibacterial properties

3.9.1 Turbidity measurement. Undoped chopped phosphate glass fibres (40-PGF), phosphate glass fibres doped with gallium (Ga-PGF) and cerium (Ce-PGF) oxide were also incubated in bacteria suspension over 48 h, and the turbidity was measured after 4, 24, and 48 h at OD 600 nm (Fig. 8). Unlike MEF and HaCaT cells used in *in vitro* studies (Sections 3.8.1 and 3.8.2), bacteria do not require the surface to attach and were incubated in direct contact with the glass fibres. All PGFs (40-PGF, Ce-PGF and Ga-PGF) showed a higher antibacterial effect against Gram-positive bacteria in the first 24 h, possibly due to the lack of outer cell membrane characteristic for this bacteria strain type. No antibacterial effect was observed against Gram-negative bacteria. The strongest antibacterial properties were measured for gallium-doped phosphate glass fibres for both Gram-positive and Gram-negative bacteria. Furthermore, no significant differences were measured between undoped fibres (P40) and Ce-PGF. The values of relative bacterial viability after 24 h were: 56%, 63% and 40% for P40-PGF, Ce-PGF and Ga-PGF, respectively. These results are in agreement with observations by other authors, showing higher antibacterial effectiveness of Ga oxide in comparison to Ce.[16]

3.10 Characterization of random PGF mesh

3.10.1 Water uptake and dissolution rate of PGF mesh in relation to wound dressing application. The results presented in Fig. 9 show increasing water uptake during 2 days of immersion in deionised water of a random mesh obtained from Ce-PGF. In the first hour, the water uptake was around 100%, followed by further water uptake (359% after 1 day and 732% after 2 days) as the mesh started to degrade. These results correspond to the water uptake capability of chitosan-based wound dressing.[65] Despite mass loss (29 ± 2% of dry mass after 2 days), the mesh kept its shape and trapped the water between the fibres. High water uptake was caused by the cotton

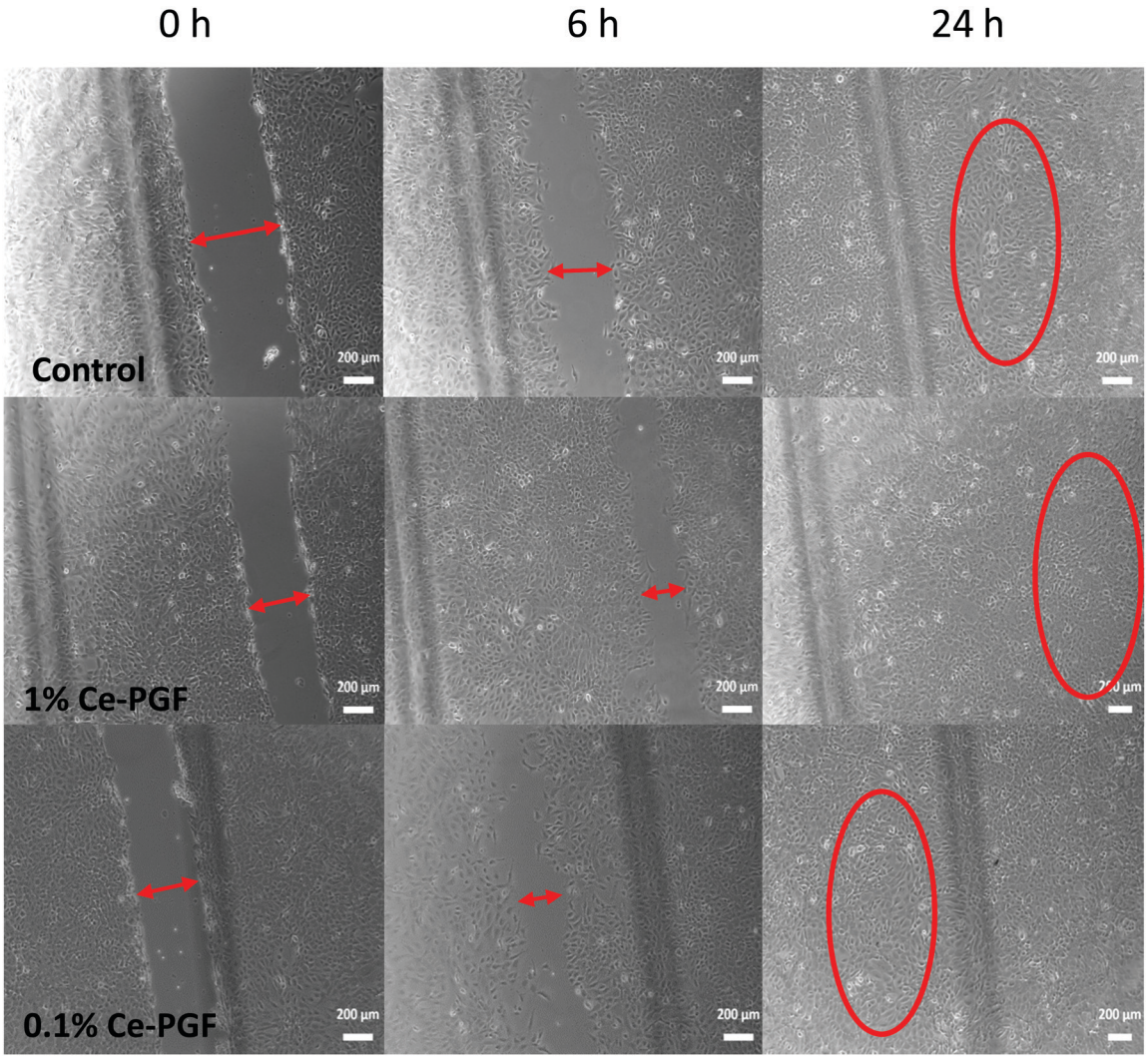

Fig. 7 Wound closure *in vitro* assay: images were taken after 0, 6 and 24 h of incubation of MEF cells in indirect contact with Ce-PGF (1 wt/vol% and 0.1 wt/vol%).

Table 5 Percentage of wound closure *in vitro* by incubation in indirect contact with 1 wt/vol% and 0.1 wt/vol% of Ce-PGF

% of wound closure					
[h]	0	4	6	8	24
Control	0%	17.38 ± 1.87%	33.93 ± 5.10%	44.92 ± 15.75%	Full closure
1% Ce PGF	0%	20.72 ± 6.83%	38.96 ± 12.46%	43.24 ± 16.72%	Full closure
0.1% Ce PGF	0%	21.76 ± 3.52%	48.66 ± 17.15%	47.19 ± 23.50%	Full closure

wool-like structure of the random mesh and the high porosity, as shown in Fig. 10.

The water soaking effect can be visualised in Fig. 11. A fragment of random mesh was placed in a 2 ml Eppendorf tube with *ca.* 0.7 ml of deionised water. The level of free water changed immediately when the mesh was soaked into the water.

Water uptake is an important feature for wound healing applications as it provides support to the moist environment of the wound.[3] It has been shown by Hinman and Maibach[66] that moist healing prevents formation of scar tissue and provides a space to drain the accumulated exudate,[67] especially in chronic wounds. A significant number of wound dressing materials are based on polymers[68] such as chitosan or alginate,[67] however, there is growing interest in applying glass-based systems.[4,6] Water uptake capability of chitosan wound dressing has been reported to be in the range 440–960%,[67] while other systems showed 200–450%[65] or only 15%.[39] Borate microfibers have been developed for wound healing applications, however, water uptake values were not reported.[7] Moreover, two products based on borate microfibers have been approved by the FDA.[4] It has been shown that a mesh structure is the most suitable for cell attachment and migration.[22]

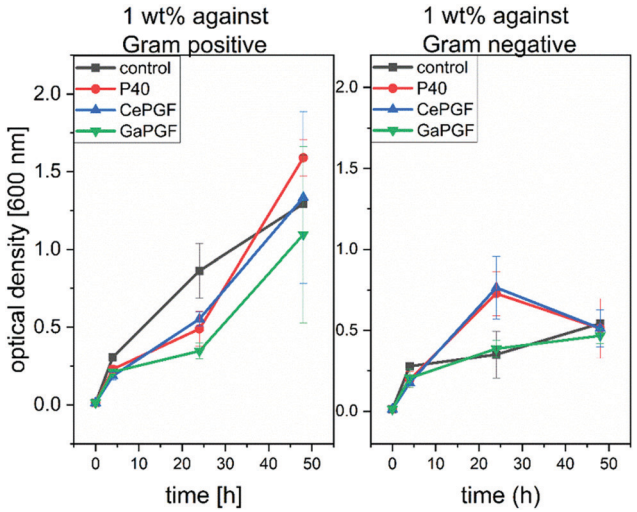

Fig. 8 OD measurement characterising the antibacterial properties of Ce-PGF, Ga-PGF and P40 against Gram-positive (left) and Gram-negative bacteria (right) after 48 h of direct incubation in bacteria suspension.

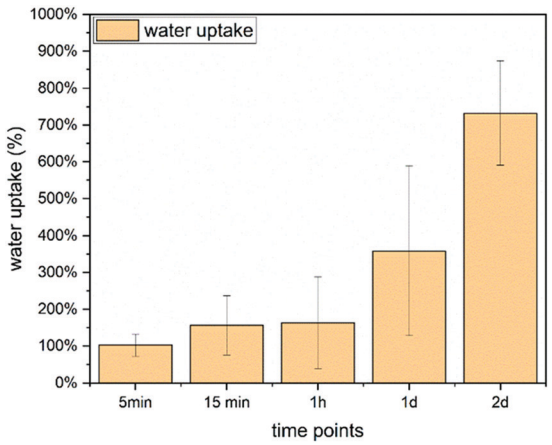

Fig. 9 Water uptake of Ce-PGF based mesh measured over 2 days, water uptake increases with time reaching 800% after 48 h.

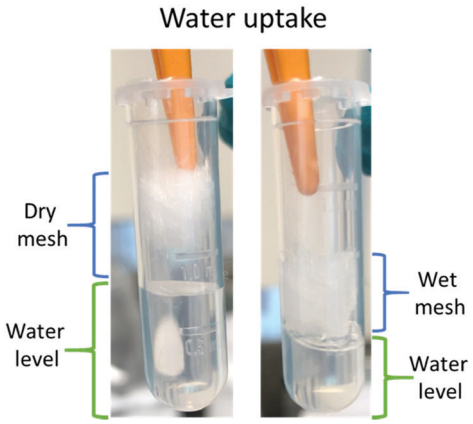

Fig. 11 Water uptake of Ce-PGF mesh – the level of water (green) decreased following immersion of the mesh.

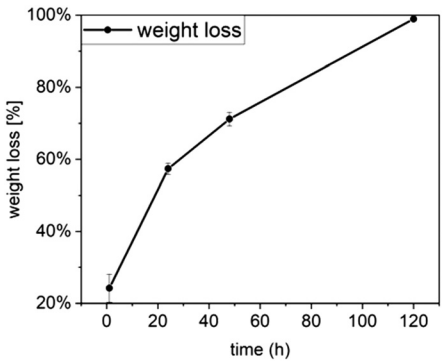

Fig. 12 Mass loss of Ce-PGF mesh over 5 days of incubation decreases significantly after 48 h.

The weight loss results presented in Fig. 12 show a significant weight loss with time, which is in agreement with the dissolution profile of Ce-PGF shown previously (Fig. 4). However, the dissolution rate of the mesh was lower than that of the fibres, which can be explained by the presence of methylcellulose used in the manufacturing process to bind

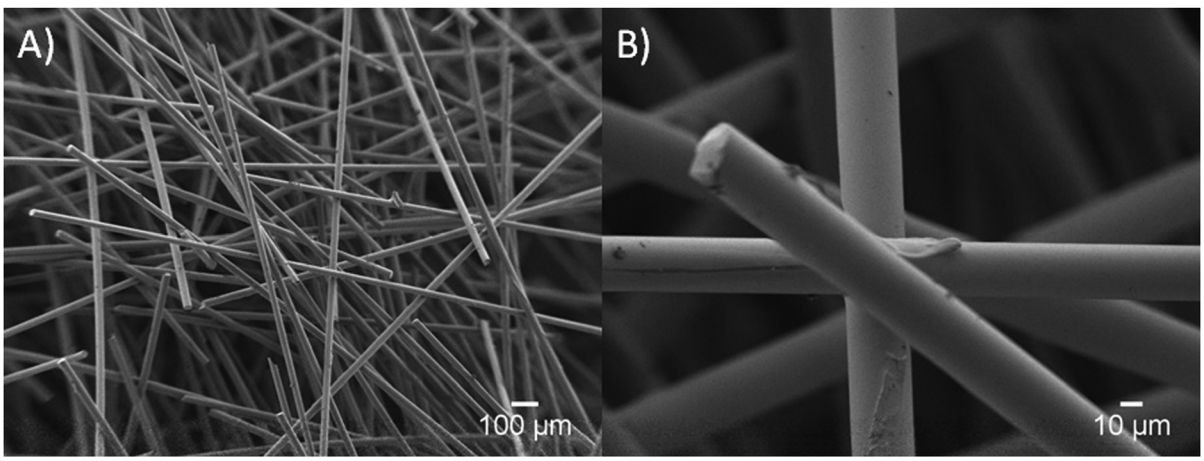

Fig. 10 SEM images of a mesh structure (A) and the connection between the Ce-PGF fibres bound by methylcellulose (B).

the fibres together. A layer of methylcellulose covered the fibres making them less accessible for water attack. High solubility of wound dressing would be beneficial as this would enable the dressing to be removed without causing further discomfort to the patient.[39]

Thus, novel Ce-PGF meshes were produced as promising wound dressing material demonstrating controlled solubility and release of therapeutic ions, high water uptake and suitable biological properties with antibacterial potential.

4. Conclusions

Novel gallium/cerium-doped phosphate-based glasses and phosphate glass fibres were successfully manufactured and characterised showing their degradation behaviour, cytocompatibility and antibacterial potential. Addition of Ga decreases the dissolution behaviour of the phosphate glass fibres, and both Ce-PGF and Ga-PGF allow for a controlled release of the ions with antibacterial properties. Due to the complex composition, more ICP measurements should be performed between 4 and 24 h of incubation, to better understand the nature and order of ions release, including assessing time variation of the ratio of ion release concentration. Moreover, solid state NMR analysis would be a powerful tool to evaluate the character of the bonding in PGF. According to the authors' best knowledge, only one type of phosphate glass fibre with antibacterial dopants has been reported in the literature,[12] which makes it impossible to compare the present results with relevant, similar systems, as they are not available. It was found that, for this composition range, only cerium-doped glasses are suited to the available continuous fibre manufacturing methods and thus they offer an interesting alternative platform for composite formation. Both cerium and gallium-doped PGF have shown mechanical properties comparable to other PGF of the same diameter. Ce-PGF random mesh was shown to be suitable for wound dressing applications due to their solubility in 4 days, antibacterial potential and good response of HaCaT cells as well as undisturbed migration of MEF cells in *in vitro* scratch assays. High degradation rates and the presence of methylcellulose may reduce the problem of painful removal of the wound dressing and high water uptake provides a moist environment, which is required to promote wound healing. Moreover, the presence and controlled release of therapeutic and antibacterial ions creates a wound dressing with the ability to reduce growth of Gram-positive bacteria by half, being non-toxic to mammal cells.

Conflicts of interest

There are no conflicts to declare.

Acknowledgements

This research was carried out as part of the HyMedPoly project, which received funding from the European Union's Horizon 2020 research and innovation program under the Marie Sklodowska-Curie grant agreement no. 643050.

References

1 J. S. Boateng, K. H. Matthews, H. N. E. Stevens and G. M. Eccleston, Wound Healing Dressings and Drug Delivery Systems: A Review, *J. Pharm. Sci.*, 2008, **97**(8), 2892–2923.
2 C. K. Sen, G. M. Gordillo, S. Roy, R. Kirsner, L. Lambert and T. K. Hunt, *et al.*, Human Skin Wounds: A Major Snowballing Threat to Public Health and Economy, *Wound Repair Regen.*, 2009, **17**(6), 763–771.
3 W. Paul and C. Sharma, Chitosan and alginate wound dressings: a short review, *Trends Biomater. Artif. Organs*, 2004, **18**(1), 18–23.
4 S. Naseri, W. C. Lepry and S. N. Nazhat, Bioactive glasses in wound healing: hope or hype?, *J. Mater. Chem. B*, 2017, **5**, 6167–6174.
5 H. Yu, J. Peng, Y. Xu, J. Chang and H. Li, Bioglass Activated Skin Tissue Engineering Constructs for Wound Healing, *ACS Appl. Mater. Interfaces*, 2016, **8**(1), 703–715.
6 V. Miguez-Pacheco, L. L. Hench and A. R. Boccaccini, Bioactive glasses beyond bone and teeth: Emerging applications in contact with soft tissues, *Acta Biomater.*, 2015, **13**, 1–15.
7 S. Zhao, L. Li, H. Wang, Y. Zhang, X. Cheng and N. Zhou, *et al.*, Wound dressings composed of copper-doped borate bioactive glass microfibers stimulate angiogenesis and heal full-thickness skin defects in a rodent model, *Biomaterials*, 2015, **53**, 379–391.
8 C. L. Ventola, The antibiotic resistance crisis: part 1: causes and threats, *P T*, 2015, **40**(4), 277–283.
9 K. Magyari, R. Stefan, D. C. Vodnar, A. Vulpoi and L. Baia, The silver influence on the structure and antibacterial properties of the bioactive 10B2O3-30Na2O-60P2O2 glass, *J. Non-Cryst. Solids*, 2014, **402**, 182–186.
10 M. Ottomeyer, A. Mohammadkah, D. Day and D. Westenberg, Broad-Spectrum Antibacterial Characteristics of Four Novel Borate-Based Bioactive Glasses, *Adv. Microbiol.*, 2016, **6**(10), 776–787.
11 J. Luo, C. Hein, F. Mücklich and M. Solioz, Killing of bacteria by copper, cadmium, and silver surfaces reveals relevant physicochemical parameters, *Biointerphases*, 2017, **12**(2), 020301.
12 E. A. Abou Neel, I. Ahmed, J. Pratten, S. N. Nazhat and J. C. Knowles, Characterisation of antibacterial copper releasing degradable phosphate glass fibres, *Biomaterials*, 2005, **26**(15), 2247–2254.
13 C. E. Albers, W. Hofstetter, K. A. Siebenrock, R. Landmann and F. M. Klenke, *In vitro* cytotoxicity of silver nanoparticles on osteoblasts and osteoclasts at antibacterial concentrations, *Nanotoxicology*, 2013, **7**(1), 30–36.
14 S. P. Valappil, D. Ready, E. A. Abou Neel, D. M. Pickup, L. A. O'Dell and W. Chrzanowski, *et al.*, Controlled delivery of antimicrobial gallium ions from phosphate-based glasses, *Acta Biomater.*, 2009, **5**(4), 1198–1210.

15 L. R. Bernstein, Mechanisms of Therapeutic Activity for Gallium, *Pharmacol. Rev.*, 1998, **50**(4), 665–682.
16 A. M. Deliormanlı, Electrospun cerium and gallium-containing silicate based 13-93 bioactive glass fibers for biomedical applications, *Ceram. Int.*, 2016, **42**(1), 897–906.
17 A. M. Deliormanlı, Synthesis and characterization of cerium- and gallium-containing borate bioactive glass scaffolds for bone tissue engineering, *J. Mater. Sci.: Mater. Med.*, 2015, **26**(2), 1–13.
18 P. Habibovic and J. E. Barralet, Bioinorganics and biomaterials: Bone repair, *Acta Biomater.*, 2011, **7**(8), 3013–3026.
19 A. Hoppe, N. S. Güldal and A. R. Boccaccini, A review of the biological response to ionic dissolution products from bioactive glasses and glass-ceramics, *Biomaterials*, 2011, **32**(11), 2757–2774.
20 V. Salih, K. Franks, M. James, G. W. Hastings, J. C. Knowles and I. Olsen, Development of soluble glasses for biomedical use part II: The biological response of human osteoblast cell lines to phosphate-based soluble glasses, *J. Mater. Sci.: Mater. Med.*, 2000, **11**(10), 615–620.
21 M. Bitar, V. Salih, V. Mudera, J. C. Knowles and M. P. Lewis, Soluble phosphate glasses: *in vitro* studies using human cells of hard and soft tissue origin, *Biomaterials*, 2004, **25**(12), 2283–2292.
22 R. Shah, A. C. M. Sinanan, J. C. Knowles, N. P. Hunt and M. P. Lewis, Craniofacial muscle engineering using a 3-dimensional phosphate glass fibre construct, *Biomaterials*, 2005, **26**(13), 1497–1505.
23 Young-Phil Kim, Gil-Su Lee, Jong-Wan Kim, Min Soo Kim, Hong-Sun Ahn, Jae-Young Lim, Hae-Won Kim, Young-Jin Son, Jonathan C. Knowles and J. K. Hyun, Phosphate glass fibres promote neurite outgrowth and early regeneration in a peripheral nerve injury model, *J. Tissue Eng. Regener. Med.*, 2015, **9**, 236–246.
24 P. Collery, B. Keppler, C. Madoulet and B. Desoize, Gallium in cancer treatment, *Crit. Rev. Oncol. Hematol.*, 2002, **42**(3), 283–296.
25 E. Verron, J. M. Bouler and J. C. Scimeca, Gallium as a potential candidate for treatment of osteoporosis, *Drug Discovery Today*, 2012, **17**(19–20), 1127–1132.
26 S. P. Valappil, D. Ready, E. A. Abou Neel, D. M. Pickup, W. Chrzanowski and L. A. O'Dell, *et al.*, Antimicrobial gallium-doped phosphate-based glasses, *Adv. Funct. Mater.*, 2008, **18**(5), 732–741.
27 F. Minandri, C. Bonchi, E. Frangipani, F. Imperi and P. Visca, Promises and failures of gallium as an antibacterial agent, *Future Microbiol.*, 2014, **9**(3), 379–397.
28 B. W. Stuart, C. A. Grant, G. E. Stan, A. C. Popa, J. J. Titman and D. M. Grant, Gallium Incorporation Into Phosphate Based Glasses: Bulk and Thin Film Properties, *J. Mech. Behav. Biomed. Mater.*, 2018, **82**, 371–382.
29 A. Cochis, B. Azzimonti, C. Della Valle, E. De Giglio, N. Bloise and L. Visai, *et al.*, The effect of silver or gallium doped titanium against the multidrug resistant Acinetobacter baumannii, *Biomaterials*, 2016, **80**, 80–95.
30 A. Rahimnejad Yazdi, L. Torkan, W. Stone and M. R. Towler, The impact of gallium content on degradation, bioactivity, and antibacterial potency of zinc borate bioactive glass, *J. Biomed. Mater. Res., Part A*, 2018, **106**(1), 367–376.
31 S. M. Rabiee, N. Nazparvar, M. Azizian, D. Vashaee and L. Tayebi, Effect of ion substitution on properties of bioactive glasses: A review, *Ceram. Int.*, 2015, **41**(6), 7241–7251.
32 F. Sayılkan, M. Asiltürk, N. Kiraz, E. Burunkaya, N. H. Ray and W. H. Huang, *et al.*, Influence of dissolution products of a novel Ca-enriched silicate bioactive glass-ceramic on VEGF release from bone marrow stromal cells, *J. Non-Cryst. Solids*, 2016, **6**(2), 9–16.
33 Y. F. Goh, A. Z. Alshemary, M. Akram, M. R. Abdul Kadir and R. Hussain, In-vitro characterization of antibacterial bioactive glass containing ceria, *Ceram. Int.*, 2014, **40**(1 Part A), 729–737.
34 S. Chigurupati, M. R. Mughal, E. Okun, S. Das, A. Kumar and M. McCaffery, *et al.*, Effects of cerium oxide nanoparticles on the growth of keratinocytes, fibroblasts and vascular endothelial cells in cutaneous wound healing, *Biomaterials*, 2013, **34**(9), 2194–2201.
35 L. M. Placek, T. J. Keenan, A. Coughlan and A. W. Wren, Investigating the Effect of Glass Ion Release on the Cytocompatibility, Antibacterial Efficacy and Antioxidant Activity of Y2O3/CeO2 doped SiO2-SrO-Na2O glasses, *Biomed. Glasses*, 2018, **4**, 32–44.
36 L. Muñoz-Senovilla, F. Muñoz, G. Tricot, I. Ahmed and A. J. Parsons, Structure–properties relationships in fibre drawing of bioactive phosphate glasses, *J. Mater. Sci.*, 2017, **52**(15), 9166–9178.
37 X. Liu, M. S. Hasan, D. M. Grant, L. T. Harper, A. J. Parsons and G. Palmer, *et al.*, Mechanical, degradation and cytocompatibility properties of magnesium coated phosphate glass fibre reinforced polycaprolactone composites, *J. Biomater. Appl.*, 2014, **29**(5), 675–687.
38 D. Gupta, C. H. Tator and M. S. Shoichet, Fast-gelling injectable blend of hyaluronan and methylcellulose for intrathecal, localized delivery to the injured spinal cord, *Biomaterials*, 2006, **27**(11), 2370–2379.
39 S. Y. Lin, K. S. Chen and L. Run-Chu, Design and evaluation of drug-loaded wound dressing having thermoresponsive, adhesive, absorptive and easy peeling properties, *Biomaterials*, 2001, **22**(22), 2999–3004.
40 N. Sharmin, A. J. Parsons, C. D. Rudd and I. Ahmed, Effect of boron oxide addition on fibre drawing, mechanical properties and dissolution behaviour of phosphate-based glass fibres with fixed 40, 45 and 50 mol% P_2O_5, *J. Biomater. Appl.*, 2014, **29**(5), 639–653.
41 S. Cereceres, T. Touchet, M. B. Browning, C. Smith, J. Rivera and M. Höök, *et al.*, Chronic Wound Dressings Based on Collagen-Mimetic Proteins, *Adv. Wound Care*, 2015, **4**(8), 444–456.
42 C. C. Liang, A. Y. Park and J. L. Guan, *In vitro* scratch assay: A convenient and inexpensive method for analysis of cell migration *in vitro*, *Nat. Protoc.*, 2007, **2**(2), 329–333.
43 L. Gritsch, C. Lovell, W. H. Goldmann and A. R. Boccaccini, Do bioresorbable polyesters have antimicrobial properties?, *J. Mater. Sci.: Mater. Med.*, 2018, **29**(2), 2–5.

44 R. C. Goy, S. T. B. Morais and O. B. G. Assis, Evaluation of the antimicrobial activity of chitosan and its quaternized derivative on E. Coli and S. aureus growth, *Rev. Bras. Farmacogn.*, 2016, **26**(1), 122–127.

45 H. Haase, L. Jordan, L. Keitel, C. Keil and B. Mahltig, Comparison of methods for determining the effectiveness of antibacterial functionalized textiles, *PLoS One*, 2017, **12**(11), 1–16.

46 K. Zheng, M. Lu, Y. Liu, Q. Chen, N. Taccardi and N. Hüser, *et al.*, Monodispersed lysozyme-functionalized bioactive glass nanoparticles with antibacterial and anticancer activities, *Biomed. Mater.*, 2016, **11**(3), 035012.

47 Y. M. Lai, X. F. Liang, S. Y. Yang, J. X. Wang, L. H. Cao and B. Dai, Raman and FTIR spectra of iron phosphate glasses containing cerium, *J. Mol. Struct.*, 2011, **992**(1–3), 84–88.

48 M. Elisa, B a Sava, I. C. Vasiliu, R. C. C. Monteiro, C. R. Iordanescu and I. D. Feraru, *et al.*, Investigations on optical, structural and thermal properties of phosphate glasses containing terbium ions, *IOP Conf. Ser.: Mater. Sci. Eng.*, 2013, **47**, 012025.

49 A. Lapa, M. Cresswell, P. Jackson and A. R. Boccaccini, Phosphate glass fibres with therapeutic ions release capability – a review, *Adv. Appl. Ceram.*, 2019, **0**(0), 1–14, DOI: 10.1080/17436753.2018.1564413.

50 R. Sahdev, T. I. Ansari, S. M. Higham and S. P. Valappil, Potential use of gallium-doped phosphate-based glass material for periodontitis treatment, *J. Biomater. Appl.*, 2015, **30**(1), 85–92.

51 J. Ren and H. Eckert, Intermediate role of gallium in oxidic glasses: Solid state NMR structural studies of the Ga2O3-NaPO3 system, *J. Phys. Chem. C*, 2014, **118**(28), 15386–15403.

52 U. Hoppe, D. Ilieva and J. Neuefeind, The structure of gallium phosphate glasses by high-energy X-ray diffraction, *Z. Naturforsch., A: Phys. Sci.*, 2002, **57**(8), 709–715.

53 N. Wantana, E. Kaewnuam, N. Chanthima, S. Kaewjaeng, H. J. Kim and J. Kaewkhao, *et al.*, Collective Optical, FTIR, and Photoluminescence Spectra of CeO2 and/or Sm2O3 Doped Na2O–ZnO–P2O5 Glasses, *J. Non-Cryst. Solids*, 2018, **44**(3), S172–S176, DOI: 10.1016/j.jnoncrysol.2013.06.016.

54 J. Belcher, J. L. Rygel, L. Kokou, C. G. Pantano, Y. Chen and R. Woodman, *et al.*, Structure of Cerium Phosphate Glasses: Molecular Dynamics Simulation, *J. Am. Ceram. Soc.*, 2011, **94**(8), 2393–2401.

55 H. Shinozaki, S. Nakashima, S. Takahashi, A. Hanada and Y. Yamamoto, Water resistance of cerium phosphate glasses as studied by in situ high temperature IR microspectroscopy, *J. Non-Cryst. Solids*, 2013, **378**, 55–60, DOI: 10.1016/j.jnoncrysol.2013.06.016.

56 C. Vitale-Brovarone, G. Novajra, J. Lousteau, D. Milanese, S. Raimondo and M. Fornaro, Phosphate glass fibres and their role in neuronal polarization and axonal growth direction, *Acta Biomater.*, 2012, **8**(3), 1125–1136.

57 E. A. Abou Neel, I. Ahmed, J. J. Blaker, A. Bismarck, A. R. Boccaccini and M. P. Lewis, *et al.*, Effect of iron on the surface, degradation and ion release properties of phosphate-based glass fibres, *Acta Biomater.*, 2005, **1**(5), 553–563.

58 I. Ahmed, M. Lewis, I. Olsen and J. C. Knowles, Phosphate glasses for tissue engineering: Part 1. Processing and characterisation of a ternary-based P2O5-CaO-Na2O glass system, *Biomaterials*, 2004, **25**(3), 491–499.

59 I. Ahmed, P. S. Cronin, E. A. Neel, A. J. Parsons, J. C. Knowles and C. D. Rudd, Retention of mechanical properties and cytocompatibility of a phosphate-based glass fiber/polylactic acid composite, *J. Biomed. Mater. Res., Part B*, 2009, **89**(1), 18–27.

60 S. Singh, A. Kumar, A. Karakoti, S. Seal and W. T. Self, Unveiling the mechanism of uptake and sub-cellular distribution of cerium oxide nanoparticles, *Mol. BioSyst.*, 2010, **6**(10), 1813–1820.

61 J. L. García, A. Asadinezhad, J. Pacherník, M. Lehocký, I. Junkar and P. Humpolíček, *et al.*, Cell Proliferation of HaCaT Keratinocytes on Collagen Films Modified by Argon Plasma Treatment, *Molecules*, 2010, **15**(4), 2845–2856.

62 R. C. Lucacel, O. Ponta, E. Licarete, T. Radu and V. Simon, Synthesis, structure, bioactivity and biocompatibility of melt-derived P2O5-CaO-B2O3-K2O-MoO3 glasses, *J. Non-Cryst. Solids*, 2016, **439**, 67–73.

63 C. Martínez-Mora, A. Mrowiec, E. M. García-Vizcaíno, A. Alcaraz, J. L. Cenis and F. J. Nicolás, Fibroin and sericin from Bombyx mori Silk stimulate cell migration through upregulation and phosphorylation of c-Jun, *PLoS One*, 2012, **7**(7), e42271.

64 M. N. M. Walter, K. T. Wright, H. R. Fuller, S. MacNeil and W. E. B. Johnson, Mesenchymal stem cell-conditioned medium accelerates skin wound healing: An *in vitro* study of fibroblast and keratinocyte scratch assays, *Exp. Cell Res.*, 2010, **316**(7), 1271–1281.

65 H. Xu, L. Ma, H. Shi, C. Gao and C. Han, Chitosan–hyaluronic acid hybrid film as a novel wound dressing: *in vitro* and *in vivo* studies, *Polym. Adv. Technol.*, 2007, **18**(11), 869–875.

66 C. D. Hinman and H. Maibach, Effect of Air Exposure and Occlusion on Experimental Human Skin Wounds, *Nature*, 1963, **200**(487), 377–378.

67 J. Y. Hao, F. L. Mi, S. S. Shyu, Y. B. Wu, J. Y. Schoung and Y. H. Tsai, *et al.*, Control of wound infections using a bilayer chitosan wound dressing with sustainable antibiotic delivery, *J. Biomed. Mater. Res.*, 2002, **59**(3), 438–449.

68 A. Zonari, T. M. M. Martins, A. C. C. Paula, J. N. Boeloni, S. Novikoff and A. P. Marques, *et al.*, Polyhydroxybutyrate-*co*-hydroxyvalerate structures loaded with adipose stem cells promote skin healing with reduced scarring, *Acta Biomater.*, 2015, **17**, 170–181.